



# Evaluation and verification of MPDZ as a prognostic biomarker for hepatocellular carcinoma through multiple databases

Jianzhu Luo<sup>1</sup> · Jianhua Liang<sup>1</sup> · Haixiang Xie<sup>2,3</sup> · Jianguang Chen<sup>1</sup> · Xiaoqiang Shen<sup>1</sup> · Fuquan Yang<sup>1</sup> · Tianman Li<sup>1</sup>

Received: 15 December 2024 / Accepted: 9 May 2025  
© The Author(s) 2025

## Abstract

The aim of this study was to assess the prognostic value of the multi-PDZ domain protein (MPDZ) in hepatocellular carcinoma (HCC). MPDZ expression in HCC and normal liver tissue samples were analyzed using TCGA-LIHC data and validated in the GSE14520, GSE62232, GSE76427, GSE121248, and GSE136247 datasets. MPDZ's prognostic value in HCC was evaluated based on Kaplan–Meier survival analysis and Cox proportional risk models. The correlation of MPDZ with other prognostic factors was explored by combined survival analysis and stratified survival analysis. The differentially expressed genes between patient groups stratified on the basis of MPDZ levels in TCGA-LIHC were screened using R and functionally annotated by the GO and KEGG pathway analysis by DAVID. Furthermore, gene set enrichment analysis was conducted to determine the basic molecular mechanism of MPDZ in HCC, and the protein–protein interactions, gene–gene interactions, and immune infiltration status of MPDZ was analyzed by STRING, GeneMania, and TIMER. Our findings indicate that MPDZ is downregulated in HCC and portends worse prognosis. Bioinformatics analysis revealed a strong link between MPDZ and liver cancer progression, liver cancer survival, multiple metabolic pathways, and multiple signaling pathways. In addition, our findings indicate that MPDZ expression is associated with several key genes in the ferroptosis pathway and m6A methylation. Finally, immunohistochemical assessment of clinical specimens confirmed low MPDZ protein expression in HCC tissues relative to paraneoplastic tissues. Taken together, MPDZ is a promising biomarker for the diagnosis and prognosis of HCC.

**Keywords** HCC<sub>1</sub> · MPDZ<sub>2</sub> · Diagnosis<sub>3</sub> · Prognosis<sub>4</sub> · Biomarker<sub>5</sub>

## Introduction

According to a new report, as many as 900,000 new liver cancer cases were diagnosed and 830,000 deaths were recorded worldwide in 2020, which currently makes liver cancer the third leading cause of cancer-related deaths [1,

2]. Liver cancer ranks the fifth of the malignancies and the second for cancer-related deaths in Asia [3]. The treatment options for hepatocellular carcinoma (HCC) include surgical resection, transarterial chemoembolization (TACE), systemic therapy, hepatic arterial infusion chemotherapy (HAIC), and liver transplantation [4]. Although immune checkpoint inhibitors have shown encouraging results against advanced HCC, the therapeutic efficacy remains to be improved [5]. The mortality rate due to HCC is increasing at the rate of about 2–3% per year [6]. If detected at an early stage, surgical resection can improve the 5-year overall survival (OS) rate of HCC patients to more than 70% [7]. On the other hand, for those with advanced liver cancer, the 5-year OS rate has declined to less than 16% [8]. Early diagnosis for HCC currently relies on ultrasound surveillance (US) and serological assessment of alpha-fetoprotein (AFP). Among HCC patients with cirrhosis regardless of the tumor stage, the diagnostic sensitivity and specificity of AFP are 41–65% and 80–94%, respectively [9], although the

✉ Tianman Li  
litianman@stu.gxmu.edu.cn

<sup>1</sup> Department of Hepatobiliary Surgery, The First People's Hospital of Yulin, No. 495, Education Middle Road, Yulin 537000, Guangxi Zhuang Autonomous Region, People's Republic of China

<sup>2</sup> Department of Hepatobiliary Surgery, The First Affiliated Hospital of Guangxi Medical University, Nanning 530021, Guangxi Zhuang Autonomous Region, People's Republic of China

<sup>3</sup> Guangxi Key Laboratory of Enhanced Recovery After Surgery for Gastrointestinal Cancer, 530021 Nanning, People's Republic of China

detection rate of early tumors is only 33% [10]. Furthermore, while the sensitivity of ultrasound imaging for HCC diagnosis is 84%, it is only 47% for the early stages [11]. Thus, sensitive biomarkers are urgently needed to diagnose HCC at the early stage and predict patient prognosis.

MPDZ, also known as MUPP1, is a multi-PDZ domain protein located on human chromosome 9p24-p22. It contains 13 PDZ structures that mediate signal transduction by binding to the C-terminus of other proteins [12]. Given its lack of an intrinsic catalytic function, MPDZ likely binds to the intercellular adhesion molecules at tight junctions [13], since it has been detected near the junctions of epithelial and endothelial cells, as well as neuronal synapses [14–16]. The choroid plexus of the central nervous system related to the expression of MPDZ [17], and it is also the main source of the cerebrospinal fluid (CSF) [18, 19]. MPDZ is in fact closely associated with congenital hydrocephalus [20]. In addition, MPDZ promotes Gi coupling and signaling at the Mt1 melatonin receptor [21], regulates p38 MAP kinase activity, enhances NMDA receptor-dependent synaptic AMPA receptor activity [22], and regulates angiogenesis by interacting with the Notch ligands DLL1 and DLL4 [23]. Recently, studies have demonstrated the pivotal role of MPDZ in tumorigenesis [24–26]. However, little is known regarding the potential regulatory functions and clinical significance of MPDZ in HCC, and the underlying mechanisms remain unclear.

## Materials and methods

### Data sources

RNA sequencing (RNA-seq) as well as the corresponding clinical data of HCC samples were retrieved from TCGA (The Cancer Genome Atlas). The gene expression data were normalized using the “limma” package scale [27]. In addition, the GSE14520, GSE62232, GSE76427, GSE121248, and GSE136247 datasets were extracted from GEO (The Gene Expression Omnibus) to validate MPDZ expression in HCC.

### ROC analysis

Receiver operating characteristic (ROC) curves were plotted to quantify MPDZ’s prognostic ability for HCC [28] by calculating the area under the curve (AUC).

### Survival analysis

HCC cases from TCGA and GSE14520 datasets were classified into the MPDZ<sup>high</sup> and MPDZ<sup>low</sup> groups according to the median expression level. Kaplan–Meier survival

curves were plotted for both groups and compared using the log-rank test. The clinicopathological characteristics obtained from TCGA and GSE14520 datasets are summarized in Tables 1 and 2. The risk values of MPDZ and individual clinicopathological features were determined by constructing a nomogram using the rms package in R, and the total risk score was calculated by summing the risk values of each variable [29]. Cox regression analysis was performed to identify the factors significantly associated with the overall survival (OS) of HCC patients. The calculation of the risk score was conducted by multiplying coefficients ( $\beta$ ) from the Cox regression model with the gene expression levels as follows:  $(\beta_1 * \text{gene 1}) + (\beta_2 * \text{gene 2}) + (\beta_3 * \text{gene 3}) + \dots + (\beta_n * \text{gene n})$  [30–32]. Since the calculated risk score was negative, the constant 5 was added to the score in TCGA and 7 was added to the score in GSE14520. Time-dependent ROC curves were drawn using the survival ROC package [30]. Survival analysis was also performed for different subgroups stratified on the basis of the clinicopathological factors.

**Table 1** Clinical profile of TCGA-LIHC patients in this study

TCGA	Low MPDZ	High MPDZ	X <sup>2</sup>	P value
<i>Age (years)</i>				
< 60	92 (0.56)	73 (0.44)	4.020	0.045
≥ 60	89 (0.45)	108 (0.55)		
Missing	0	0		
<i>Histologic grade</i>				
G1 + G2	95 (0.41)	135 (0.59)	20.190	< 0.001
G3 + G4	84 (0.66)	43 (0.34)		
Missing	2	3		
<i>Gender</i>				
Female	66 (0.56)	52 (0.44)	2.464	0.116
Male	115 (0.47)	129 (0.53)		
Missing	0	0		
<i>Race</i>				
Asian	94 (0.60)	62 (0.40)	13.193	0.001
Black	7 (0.44)	9 (0.56)		
White	73 (0.41)	107 (0.59)		
Missing	7	3		
<i>Tumor stage</i>				
Stage I and II	121 (0.48)	132 (0.52)	3.773	0.052
Stage III and IV	51 (0.60)	34 (0.40)		
Missing	9	15		
<i>BMI (kg/m<sup>2</sup>)</i>				
< 18.5	15 (0.71)	6 (0.29)	12.610	0.006
18.5–24.9	85 (0.55)	69 (0.45)		
25–29.9	45 (0.51)	43 (0.49)		
≥ 30	23 (0.34)	45 (0.66)		
Missing	13	18		

**Table 2** Clinical profile of patients in this study from the GSE14520 database

GSE14520	Low MPDZ	High MPDZ	X <sup>2</sup>	P value
<i>Gender</i>				
Female	12 (0.41)	17 (0.59)	0.999	0.318
Male	94 (0.51)	89 (0.49)		
Missing	0	0		
<i>Age (years)</i>				
<60	95 (0.55)	77 (0.45)	9.984	0.002
60	11 (0.28)	29 (0.72)		
Missing	0	0		
<i>Main tumor size</i>				
≤5CM	65 (0.47)	72 (0.53)	1.218	0.270
>5CM	41 (0.46)	33 (0.54)		
Missing	0	1		
<i>Multinodular</i>				
Yes	29 (0.64)	16 (0.36)	4.768	0.029
No	77 (0.46)	90 (0.54)		
Missing	0	0		
<i>Cirrhosis</i>				
Yes	98 (0.50)	97 (0.50)	0.064	0.800
No	8 (0.50)	9 (0.50)		
Missing	0	0		
<i>AFP</i>				
≤300 ng/ml	43 (0.37)	72 (0.63)	16.833	<0.001
>300 ng/ml	62 (0.66)	32 (0.34)		
Missing	1	2		

AFP alpha-fetoprotein

### HPA analysis

The Human Protein Atlas (HPA, <https://www.proteinatlas.org/>) is a database of immunohistochemical (IHC) images of specimens from a wide range of cancers [33]. The IHC images for MPDZ in HCC tissues were downloaded from HPA.

### PPI network analysis

The STRING database was used to build the protein–protein interaction (PPI) network [34] for MPDZ. The interactions with a composite score > 0.4 were defined as statistically significant.

### GeneMANIA analysis

The GeneMANIA website was used for the prediction MPDZ's function as well as the identification of genes with similar functions in HCC [35].

### Immune infiltration analysis

The tumor immune estimation resource (TIMER) algorithm was used to analyze the infiltration of six immune cell types in HCC and their correlation with MPDZ expression.

### Gene set enrichment analysis (GSEA)

The pathways and functions associated with MPDZ were identified through c2 (c2.all.v7.5.1.symbols.gmt) and c5 (c5.all.v7.5.1.symbols.gmt) molecular signature database (MSigDB) in GSEA 4.2.3 [36]. TCGA-LIHC patients were allocated into the MPDZ<sup>high</sup> group or the MPDZ<sup>low</sup> group based on the median expression. GSEA-derived gene enrichment groups with FDR < 0.25 and *P* < 0.05 with an alignment parameter set to 1,000 were considered statistically significant.

### Identification of differentially expressed genes (DEGs)

The DEGs between the MPDZ<sup>high</sup> and MPDZ<sup>low</sup> TCGA-LIHC were screened using the R package LIMMA, with the criteria of  $|\log_2(\text{Fold Change})| > 1.5$  and *P* < 0.05. The DEGs were visualized in the form of a volcano plot using the ggplot2 package.

### Functional annotation

The analyses of Gene Ontology (GO) [37] as well as Kyoto Encyclopedia of Genes and Genomic Pathways (KEGG) [38] of DEGs were carried out using Database for Annotation, Visualization, and Integrated Discovery (DAVID). The enriched biological functions and pathways were visualized by "Goplot, Hmisc, and ggplot2".

### Immunohistochemistry

After cut into sections (4 μm thick), the paraffin-embedded tissues were dewaxed in xylene and then hydrated through an ethanol gradient (100%, 95%, 85%, and 75%). The sections were heated in 0.1 M citrate buffer (pH-6.0) at 95 °C for 15 min to unmask the antigens, and thereafter immersed in 0.3% H<sub>2</sub>O<sub>2</sub> for 20 min at room temperature to block the endogenous peroxidase activity. The slides were incubated overnight with the primary antibody (Affinity, USA) at 4 °C, followed by the secondary antibody (ZSGB-Bio, China) at 37 °C for 30 min, and the Detection System PV-9000 (ZSGB-Bio, China) at 37 °C for 20 min. After developing color with the diaminobenzidine (DAB) solution (Dako, Denmark), the sections were counterstained with hematoxylin solution. The slides were evaluated independently by two pathologists in a blinded manner. The staining intensity was

scored as follows: (1) 0: negative staining; (2) 1: light staining; (3) 2: brown; and (4) 3: tan. The percentage of positive cells was scored as follows: (1) 1: 0–10%; (2) 2: 10–50%; (3) 3: 50–75%; and (4) 4: 75–100%. Both scores were multiplied, and the samples were classified on the basis of the total score as high expression  $\geq 4$  and low expression  $< 4$ .

## DNA methylation

To analyze MPDZ and the relationship between DNA methylation in HCC, this study adopts MethSurv platform to explore (<https://biit.cs.ut.ee/methsurv/>), which is a survival analysis of DNA methylation patterns of effective tools [39].

## Statistical analysis

SPSS version 25.0 and R (version 4.2.0) as well as GraphPad Prism 8.0 were used for statistical analyses. Differential gene expression of the normal and tumor tissues was compared by Student's *t* test. Chi-square or Fisher's exact test was used to investigate the relationship of MPDZ gene expression with clinicopathological features. Univariate and multifactorial Cox proportional risk regression models were applied to identify the prognostic value of various clinical features. A *P* value  $< 0.05$  indicated statistical significance.

## Results

### MPDZ is downregulated in HCC

Analysis of pan-cancer datasets in TIMER revealed higher expression of MPDZ in 15 tumor types compared to the corresponding normal tissue (Fig. 1A). However, MPDZ was significantly downregulated in the HCC tissues compared to the normal liver tissues in TCGA-LIHC database ( $P < 0.0001$ ; Fig. 1B). Consistent with this, lower MPDZ mRNA levels were detected in the liver cancer tissues in the GSE14520, GSE136247, GSE76427, GSE62232, and GSE121248 datasets (Fig. 1C–G). The diagnostic efficacy of MPDZ was evaluated by ROC analysis, and AUC was greater than 0.8 in all examined datasets (TCGA = 0.8665, GSE14520 = 0.8783, GSE136247 = 0.8850, GSE76427 = 0.6987, GSE62232 = 0.8086, GSE121248 = 0.7386), indicating that MPDZ expression can accurately diagnose HCC (Fig. 1H–M). MPDZ protein expression was also lower in HCC tissues than in normal liver tissues as per HPA data (Fig. 2A). In contrast to the corresponding normal tissues, the protein expression of MPDZ in hepatocellular carcinoma tissues was lower according to immunohistochemistry (Fig. 2B–E).

### MPDZ is a prognostic factor in HCC

Higher MPDZ mRNA expression was significantly related to better OS ( $P = 0.0024$  in TCGA, Fig. 2E;  $P = 0.0012$  in GSE14520, Fig. 2F). Furthermore, multivariate Cox proportional hazards regression identified MPDZ as an independent prognostic factor in TCGA ( $P = 0.002$ , 95% CI 0.383–0.814, Table 3) and GSE14520 ( $P = 0.005$ , 95% CI 0.312–0.816, Table 4) datasets. Time-dependent ROC curves confirmed the Kaplan–Meier survival analysis with respective AUC values of 0.5813 (95% CI 0.5184–0.6441) and 0.6252 (95% CI 0.5468–0.7037) in TCGA and GSE14520 datasets (Fig. 2G, H). GSE136247, GSE76427, GSE62232, and GSE121248 were not included in the analysis due to missing survival data.

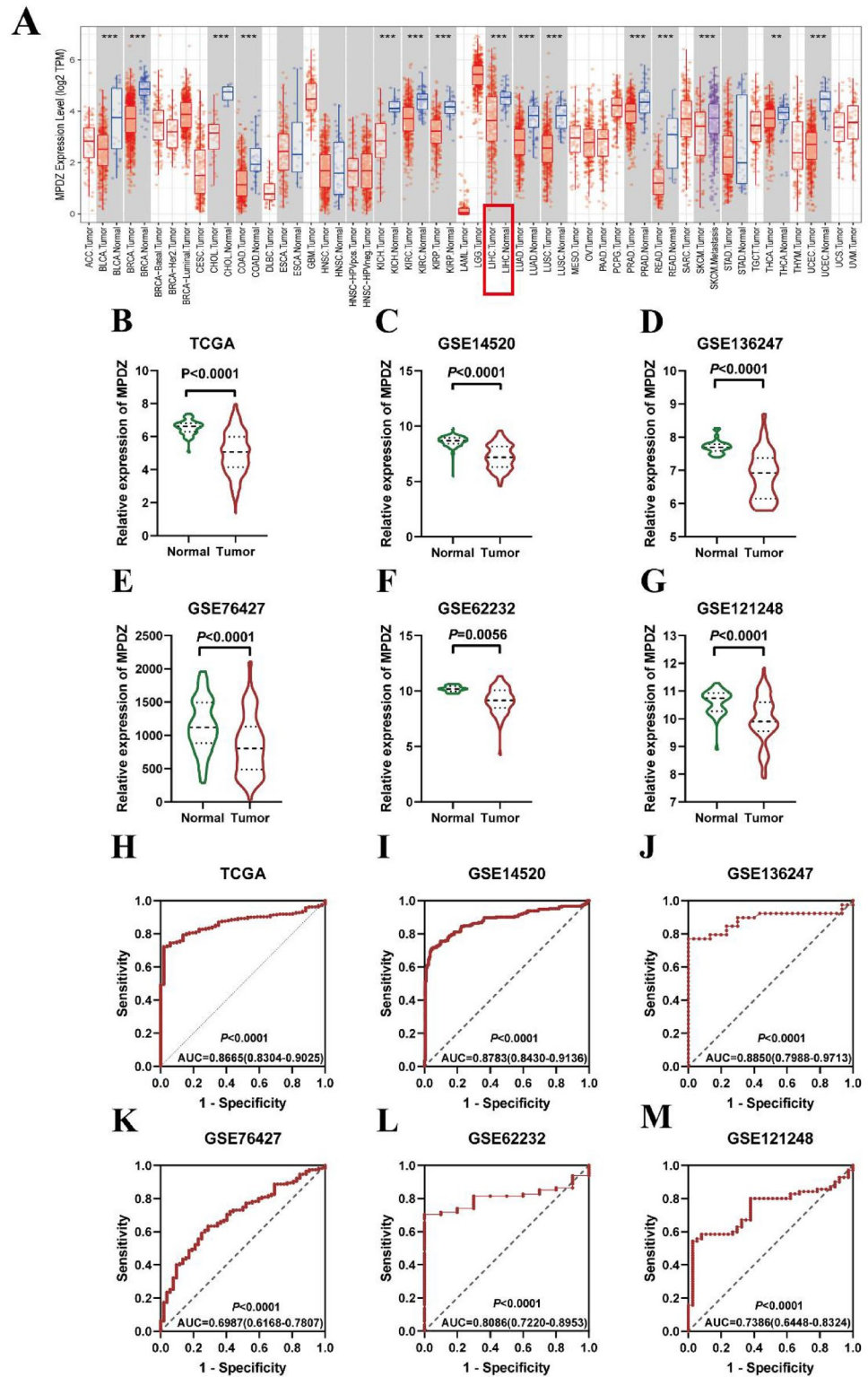
The data from TCGA and GSE14520 were used for constructing a prognostic nomogram. As shown in Fig. 3A, B, low MPDZ expression significantly correlated to worse prognosis in TCGA and GSE14520. The patients in both cohorts were then classified into the high and low risk groups based on the risk score of the nomogram. In TCGA, the risk score's AUC for the prediction of 1-, 3-, and 5-year OS among HCC patients was found to be 0.598, 0.595, and 0.607, respectively (Fig. 4A), and 0.618, 0.578, and 0.56 in GSE14520 (Fig. 4B).

Furthermore, the combination of low MPDZ expression and tumor stage III/IV was correlated to worse OS compared to the other three groups in TCGA ( $P < 0.001$ , HR = 3.388, 95% CI 2.096–5.476, Fig. 5A, Table 5). Finally, stratified survival analysis on the basis of clinicopathological features in TCGA showed that MPDZ expression was significantly correlated to the OS in the  $< 60$  years, histological tumor grade G1 + G2, female, Asian, tumor stage III and IV, and BMI 18.5–29.9 subgroups (Table 6).

### Screening and biological function of DEGs

Based on the median MPDZ mRNA expression, 362 HCC patients in TCGA were classified into either the high or low expression group. We identified 176 DEGs between the two groups, of which 162 genes were upregulated and 17 genes were downregulated (Fig. 5B). The DEGs were functionally annotated by GO and KEGG pathway analyses (Fig. 5C, D). KEGG enrichment results showed that the DEGs are associated with steroid hormone biosynthesis, metabolic pathways, retinol metabolism, primary bile acid biosynthesis, tyrosine metabolism, glycolysis/gluconeogenesis, and PPAR signaling pathway (Fig. 5E). In addition, the significantly enriched GO terms associated with DEGs included drug metabolic processes, monooxygenase activity, iron ion binding, cyclooxygenase P450 pathway, retinol metabolic processes, oxidoreductase activity, and estrogen metabolic processes (Fig. 5F).

**Fig. 1** A MPDZ mRNA expression levels in a variety of tumor tissues and normal liver tissues. \*\*\* $P < 0.001$ , \*\* $P < 0.01$ . B–G MPDZ mRNA expression in hepatocellular carcinoma tissues and normal liver tissues in six databases and (H–M) their ROC curve



### Identification of prognostic DEGs

The top 10 upregulated and downregulated genes were screened from the DEGs identified in TCGA. As shown in Fig. 6A, all 20 genes were found to be differentially

expressed between HCC and normal liver tissues. Besides, the expression of SLC10A1, ADH4, CYP3A4, CYP8B1, TAT, TESK, and SPP1 was related to HCC patients' OS with statistical significance (Fig. 6B).

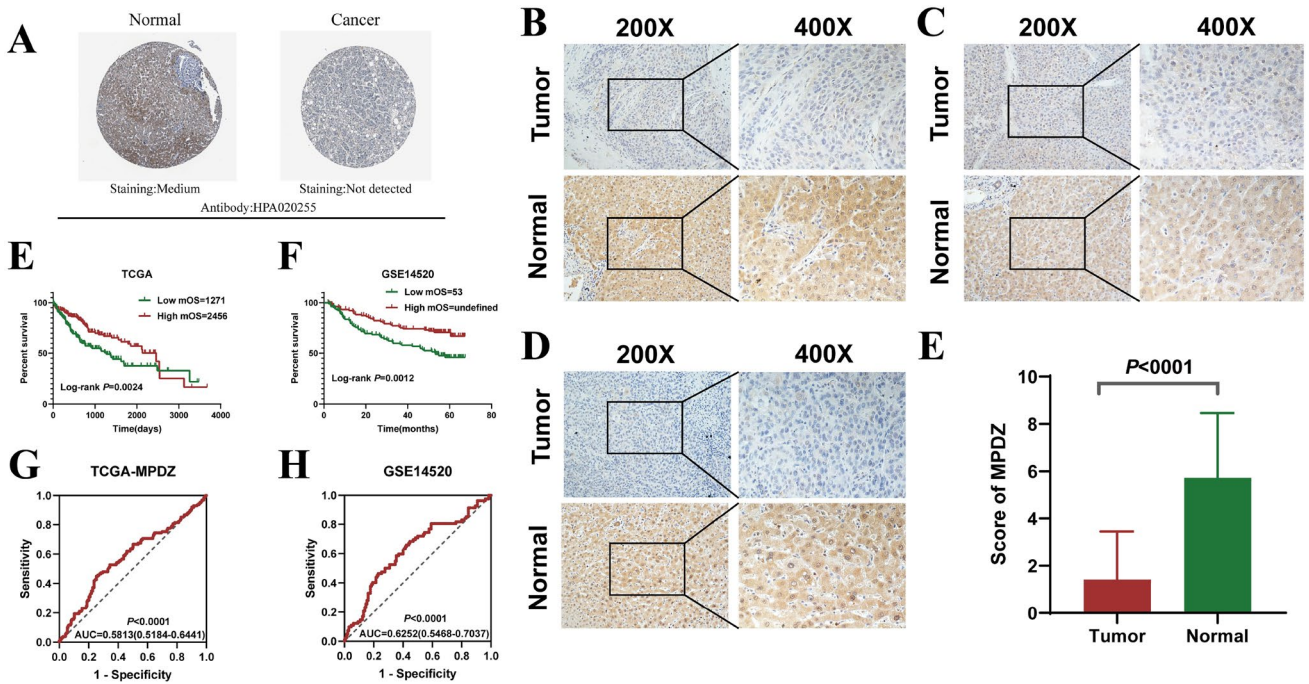


**Fig. 2** A Representative immunohistochemical images of MPDZ in HPA; **B–D** Representative immunohistochemical images of MPDZ and **D** corresponding histograms; Kaplan–Meier survival curves (**E**) and ROC curves (**G**) of MPDZ in TCGA; and Kaplan–Meier survival curves (**F**) and ROC curves (**H**) of MPDZ in GSE14520

and ROC curves (**G**) of MPDZ in TCGA; and Kaplan–Meier survival curves (**F**) and ROC curves (**H**) of MPDZ in GSE14520

## Bioinformatics analysis

The key genes involved in HCC development were identified using GeneMANIA and STRING. The PPI network indicated that the MPDZ gene was mainly co-expressed with MPP5, CSPG4, SYNGAP, PLEKHG5, PLEKHA1, HTR2C, AMOT, GRIN2B, IER5, FAT4, AMOTL1, SSTR3, CRB1, KIT, and AMOTL2 (Fig. 7A). The gene–gene relationship network generated by GeneMANIA showed that MPDZ is associated with F11R, CLDN1, PLEKHA1, HTR2C, SSTR3, CSPG4, CXADR, RIMS2, LIN7C, TEAD2, and CLDN5 (Fig. 7B). In addition, the TIMER algorithm showed that MPDZ correlated positively with the infiltration of CD4 + T cells, B cells, macrophages, CD8 + T cells, dendritic cells, and neutrophils (Fig. 7C). To investigate the correlation between MPDZ expression and immune infiltration, we determined the enrichment scores of 23 immune cells in the MPDZ expression low/high group. Our findings showed that a higher enrichment score for ten immune cells and a lower enrichment score for five immune cells were observed in the low MPDZ expression group compared to the high MPDZ expression group. We observed a negative correlation between SARDH expression and levels of infiltration of ten immune cells, but a positive correlation between SARDH expression and levels of infiltration of five immune cells (Fig. 7D–F).

## GSEA

The MPDZ<sup>high</sup> group was significantly enriched in AKT pathway, PPAR signaling pathway, MTOR pathway, hepatocellular carcinoma progression, hepatocellular carcinoma survival, and vascular invasion in HCC from the c2 reference gene set (Fig. 8A–F). The results of the c7 reference gene set showed significant enrichment of bile acid and bile salt transport, fat oxidation, negative regulation of TOR signaling, regulation of fatty acid metabolic processes, regulation of gluconeogenesis, and steroid biosynthesis (Fig. 8G–L).

## Ferroptosis pathway

Ferroptosis has been found to have a critical effect on HCC development [40–42]. To further explore the association between MPDZ expression and 25 genes involved in the ferroptosis pathway, we analyzed RNA-seq data from TCGA database [43]. The results showed that MPDZ expression was negatively correlated with five genes in the ferroptosis pathway and positively correlated with eight genes (Fig. 9).

## Methylation

To further explore the association between MPDZ expression and 24 genes involved in the ferroptosis pathway [44], we analyzed RNA-seq data from TCGA database.

**Table 3** COX regression analysis for OS in HCC patients from TCGA

Variable	Patients (n = 362)	No. of events	MST (days)	Univariate analysis		Multivariate analysis	
				HR (95%CI)	P value	HR (95%CI)	P value
<i>Age (years)</i>							
< 60	165	54	2116	1			
≥ 60	197	75	1622	1.216 (0.857–1.727)	0.273		
Missing	0	0					
<i>Histologic grade</i>							
G1 + G2	230	78	1791	1			
G3 + G4	127	47	1622	1.122 (0.780–1.612)	0.535		
Missing	5	4					
<i>Gender</i>							
Female	118	50	1560	1			
Male	244	79	2486	0.825 (0.578–1.178)	0.290		
Missing	0	0					
<i>Race</i>							
Asian	156	44	NA	1			
Black	16	6	1149	1.558 (0.663–3.659)	0.309		
White	180	74	1386	1.306 (0.896–1.904)	0.165		
Missing	10	5					
<i>Tumor stage</i>							
I and II	253	68	2532	1			
III and IV	85	47	660	2.484 (1.709–3.609)	<0.001	2.558 (1.758–3.721)	<0.001
Missing	24	14					
<i>BMI (kg/m<sup>2</sup>)</i>							
< 18.5	21	6	3258	1			
= 18.5–24.9	154	55	1694	1.529 (0.647–3.614)	0.333		
= 25–29.9	88	28	2131	1.131 (0.465–2.752)	0.786		
≥ 30	68	23	2116	1.269 (0.508–3.171)	0.610		
Missing	31	17					
<i>MPDZ</i>							
Low expression	181	77	1271	1			
High expression	181	52	2456	0.583 (0.410–0.830)	0.003	0.558 (0.383–0.814)	0.002
Missing	0	0					

HCC, hepatocellular carcinoma; MST, median survival time; OS, overall survival; HR, hazard ratio; CI, confidence interval

The results showed that MPDZ expression was negatively correlated with three genes in the m6A methylation and positively correlated with 12 genes (Fig. 10).

A comprehensive examination of the prognostic relevance of DNA methylation levels and intragenic CpG islands of the MPDZ gene was performed using the MethSurv database. The results showed that the majority of these CpG sites exhibited hypermethylation. Specifically, two CpG sites cg14404301 and cg22117143 showed that the DNA methylation level was correlated with the prognosis of HCC (Fig. 11).

## Discussion

MPDZ expression among HCC/normal liver tissues was analyzed using TCGA-LIHC dataset [45] and validated the results in GSE14520, GSE136247, GSE76427, GSE62232, and GSE121248 datasets in this study. In contrast to the normal tissues, MPDZ was found to be downregulated in HCC tissues; thus, it was identified as a tumor suppressor. Furthermore, MPDZ showed high diagnostic efficacy for HCC in GSE76427 (AUC = 0.6987) and GSE121248

**Table 4** COX regression analysis for OS in HCC patients from GSE14520

Variable	Patients (n = 212)	No. of events	MST (months)	Univariate analysis		Multivariate analysis	
				HR (95%CI)	P value	HR (95%CI)	P value
<i>Gender</i>							
Female	29	8	NA	1			
Male	183	74	NA	1.704 (0.821–3.534)	0.152		
Missing	0	0					
<i>Age (years)</i>							
<60	172	69	NA	1			
≥60	40	13	NA	0.761 (0.420–1.376)	0.366		
Missing	0	0					
<i>Main tumor size</i>							
Small	137	46	NA	1			
Large	74	36	53.3	1.925 (1.222–3.031)	0.002	1.137 (0.680–1.902)	0.005
Missing	1	0					
<i>Multinodular</i>							
Yes	45	23	NA	1			
No	167	59	47.9	1.607 (0.992–2.604)	0.054		
Missing	0	0					
<i>Cirrhosis</i>							
Yes	195	80	NA	1			
No	17	2	NA	4.335 (1.065–17.638)	0.041	4.281 (1.049–17.469)	0.043
Missing	0	0					
<i>AFP</i>							
Low	115	39	NA	1			
High	94	43	NA	1.546 (1.002–2.385)	0.049	1.086 (0.674–1.750)	0.734
Missing	3	0					
Missing	0	0					
<i>MPDZ</i>							
Low expression	181	52	53.3	1			
High expression	181	30	NA	0.484 (0.309–0.759)	0.002	0.505 (0.312–0.816)	0.005
Missing	0	0					

HCC, hepatocellular carcinoma; MST, median survival time; OS, overall survival; HR, hazard ratio; CI, confidence interval, AFP, alpha-fetoprotein

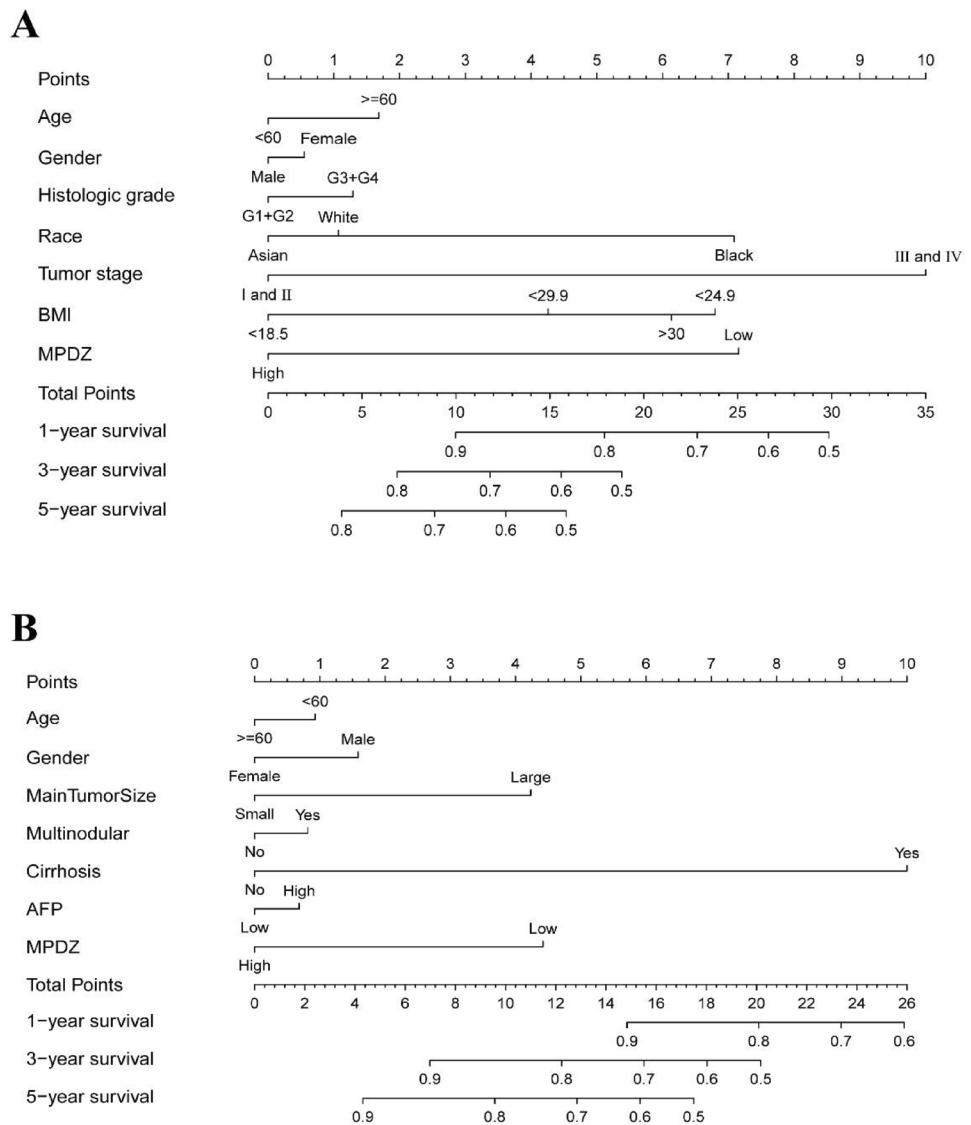
(AUC = 0.7386) datasets, and therefore can be considered as a potential diagnostic marker.

A high expression of MPDZ was related with a better OS in TCGA-CIHC and GSE14520 datasets including a total of 474 cases. In addition, MPDZ had a greater contribution to HCC prognosis in the nomogram including multiple clinicopathological characteristics for both datasets. The combination of MPDZ and tumor stage resulted in greater prognostic differences between the groups in TCGA-LIHC dataset. Furthermore, stratified survival analysis confirmed the prognostic relevance of MPDZ in the <60 years, histological grade G1 + G2, female, Asian, tumor stage III/IV and BMI 18.5–29.9 subgroups. MPDZ expression also correlated positively with the infiltration of immune cells. Given the promising results obtained with immune checkpoint inhibitors (ICIs) against liver

cancer [46], and the importance of the tumor immune landscape in therapeutic responses [47, 48], we can surmise that MPDZ may regulate HCC progression by modulating immune cell infiltration.

MPDZ is a signal transduction protein that binds to multiple proteins or protein complexes. Recent studies have shown that MPDZ is strongly correlated with alcohol addiction [49], hydrocephalus [16, 20], epilepsy susceptibility [50], other neuropathies, and even cancer. Liu et al. reported that MPDZ inhibits lung carcinogenesis by regulating the Hippo-YAP signaling pathway [51]. Furthermore, Huang et al. showed that MPDZ is a potential biomarker for early diagnosis and prognosis among patients with clear cell renal cell carcinoma [52]. A recent study associated mutations in MPDZ with drug resistance and relapse in glioblastoma patients [53].

**Fig. 3** Nomograph integrating MPDZ expression and clinico-pathological features. **A** TCGA and **B** GSE14520



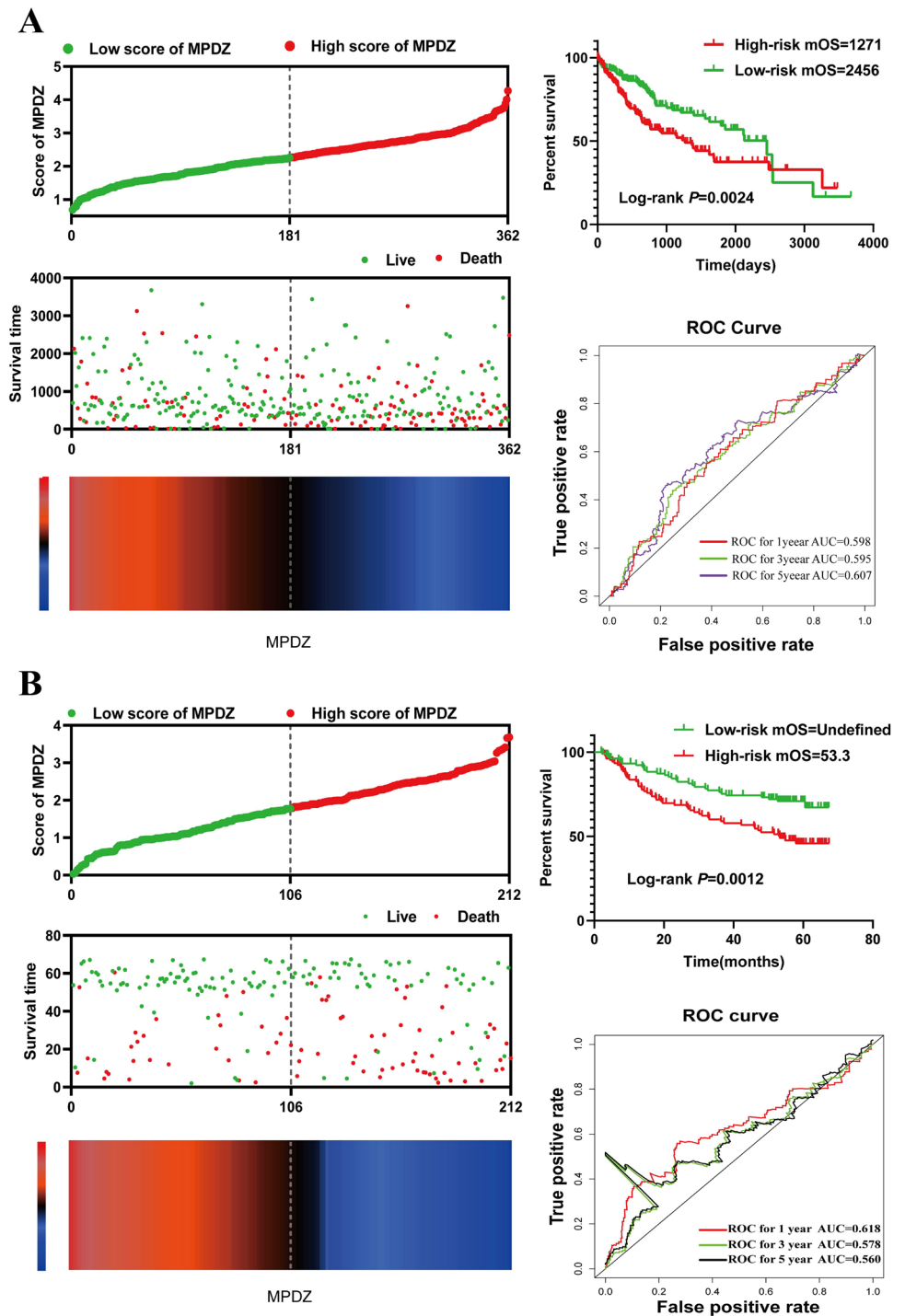
GO and KEGG enrichment analysis revealed that MPDZ was associated with the biosynthesis of steroid hormone biosynthesis/primary bile acid, PPAR signaling pathway, tyrosine metabolism, glycolysis/gluconeogenesis, drug metabolic processes, steroid metabolic processes, monoxygenase activity, cyclooxygenase pathway, retinol metabolic processes, oxidoreductase activity, and estrogen metabolic processes. The PPAR signaling pathway [54], cyclooxygenase pathway [55], and oxidoreductase activity [56] have been found to exert a pivotal impact on the development of hepatocarcinoma. In addition, PPAR signaling [57] and tyrosine metabolism [58] are strongly related to drug resistance in HCC patients. The results of GSEA further showed that MPDZ was significantly enriched in biological functions such as fat oxidation [59], negative regulation of TOR signaling [60], regulation of fatty acid metabolic processes [61], regulation of gluconeogenesis [62], transport of bile

acids and bile salts [63], AKT pathway [64], PPAR signaling pathway [57], and HCC progression, survival, and vascular invasion, which confirm that MPDZ is strongly associated with the development of hepatocellular carcinoma.

Recent investigations have revealed that ferroptosis plays a crucial role in the progression of HCC [65]. No studies have explored the potential regulatory mechanisms of MPDZ and ferroptosis pathway. In this study, we explored the relationship between MPDZ and ferroptosis in HCC using bioinformatics methods based on TCGA database. Our results showed that MPDZ expression was negatively correlated with five genes in the ferroptosis pathway and positively correlated with eight genes. MPDZ may be involved in the regulation of ferroptosis to affect the survival and progression of HCC cells.

Increasing evidence has suggested that epigenetic changes by DNA methylation and m6A methylation play an

**Fig. 4** Prognostic risk model for MPDZ in hepatocellular carcinoma. **A** TCGA and **B** GSE14520



important role in HCC [66, 67]. Recent studies have shown that MPDZ expression is regulated by CpG island hypermethylation, MPDZ expression is significantly downregulated in lung cancer tissues, negatively correlated with DNA hypermethylation, and reduced MPDZ expression predicts poor outcome [51]. In this study, two CpG sites cg14404301 and cg22117143 showed that the DNA methylation level was correlated with the prognosis of HCC. In addition,

MPDZ expression of HCC was negatively correlated with three genes in the m6A methylation and positively correlated with 12 genes.

Our study has some limitations that ought to be considered. First, both TCGA and GSE14520 datasets have incomplete clinical information, which may affect the credibility of our results. Second, additional functional experiments are needed to verify the biological function of MPDZ. Finally,

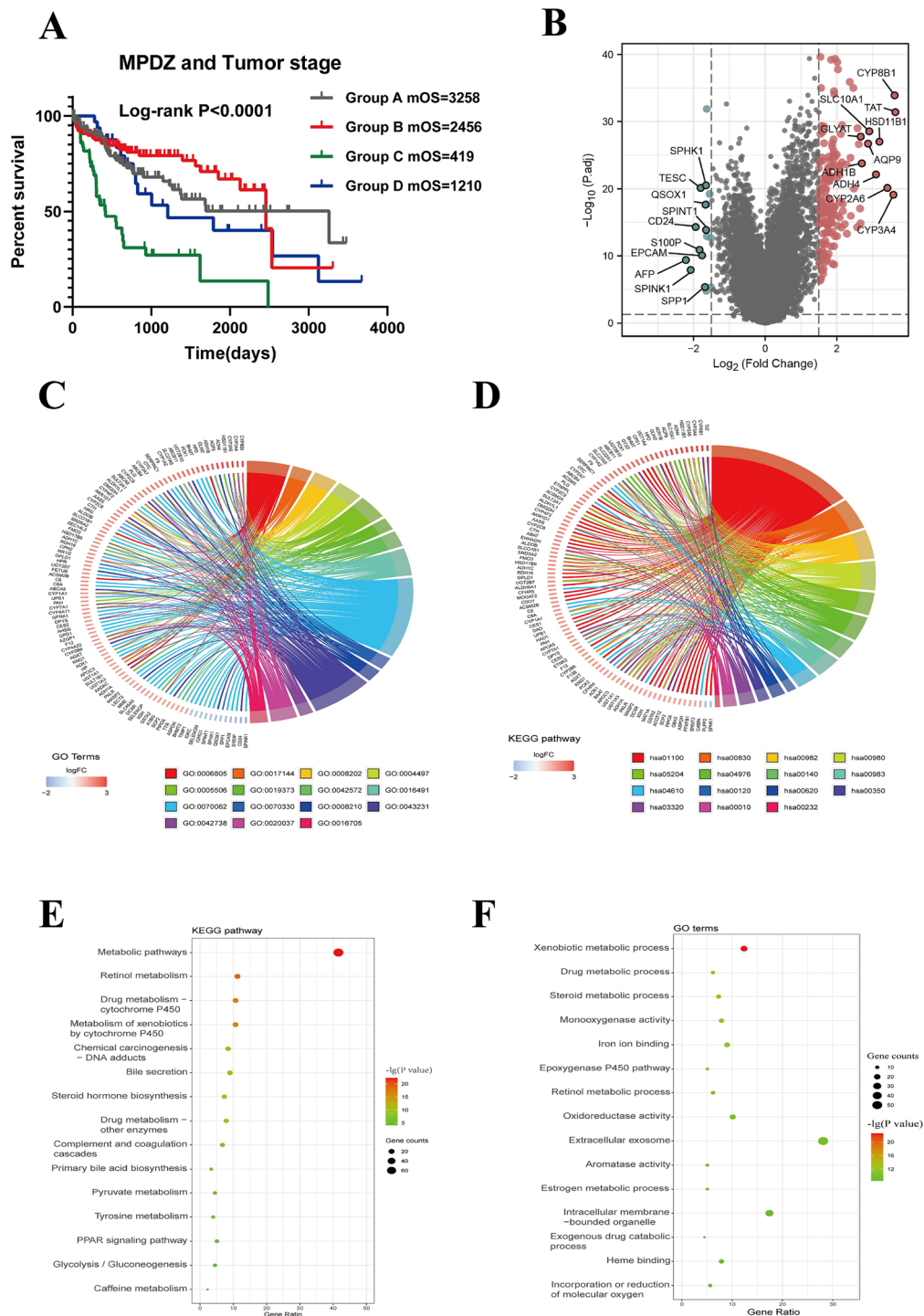


**Fig. 5** **A** Kaplan–Meier survival curves for the combined role of MPDZ and tumor stage in hepatocellular carcinoma from the TCGA database; **B** volcano plot of DEGs. Red dots: upregulated; green dots: downregulated; black dots: non-differentially expressed genes; gene names: the 10 most significantly upregulated genes and the 10 most

significantly downregulated genes in expression screened according to  $|\log_2(\text{Fold Change})|$ . **C** Circle plot for displaying the relationship between gene and GO terms; **D** circle plot for displaying the relationship between gene and KEGG pathway; **E** bubble plot for GO terms, and **F** bubble plot for KEGG pathway

we based our conclusions solely on retrospective data, and the clinical relevance of MPDZ will have to be ascertained through multicenter studies. In conclusion, we have reported

the prognostic value of MPDZ in HCC for the first time, and MPDZ warrants further investigation as a biomarker for the diagnosis and prognosis of HCC.

**Table 5** Combined effect survival analysis of tumor stage and MPDZ

Group	Tumor stage	MPDZ	Patients	No. of events	MST (days)	Univariate analysis (95% CI)	<i>P</i> value
A	I and II	Low	121	38	3258	1	-
B	I and II	High	132	30	2456	0.741 (0.458–1.199)	0.222
C	III and IV	High	51	32	419	3.388 (2.096–5.476)	<0.001
D	III and IV	Low	34	15	1210	1.220 (0.670–2.222)	0.515

MST, median survival time; No. of events, number of events; HR, hazard ratio; CI, confidence interval

**Table 6** Stratified analysis of MPDZ for OS in HCC from TCGA

TCGA	Low MPDZ	High MPDZ	Crude HR (95% CI)	Crude <i>P</i> value	Adjusted* HR (95%CI)	Adjusted* <i>P</i> value
<i>Age (years)</i>						
< 60	92 (0.56)	73 (0.44)	0.378 (0.210–0.680)	0.001	0.306 (0.160–0.585)	<0.001
≥ 60	89 (0.45)	108 (0.55)	0.795 (0.502–1.259)	0.329	0.838 (0.514–1.366)	0.487
Missing	0	0				
<i>Histologic grade</i>						
G1 + G2	95 (0.41)	135 (0.59)	0.588 (0.376–0.921)	0.020	0.561 (0.346–0.910)	0.019
G3 + G4	84 (0.66)	43 (0.34)	0.506 (0.257–0.994)	0.048	0.519 (0.256–1.052)	0.069
Missing	2	3				
<i>Gender</i>						
Female	66 (0.56)	52 (0.44)	1.111 (0.633–1.952)	0.714	1.843 (0.986–3.443)	0.459
Male	115 (0.47)	129 (0.53)	0.408 (0.257–0.648)	<0.001	0.345 (0.208–0.572)	<0.001
Missing	0	0				
<i>Race</i>						
Asian	94 (0.60)	62 (0.40)	0.218 (0.097–0.489)	<0.001	0.242 (0.107–0.548)	0.001
Black	7 (0.44)	9 (0.56)	0.440 (0.072–2.671)	0.372	0.792 (0.132–4.767)	0.799
White	73 (0.41)	107 (0.59)	0.897 (0.566–1.420)	0.643	0.932 (0.832–2.370)	0.782
Missing	7	3				
<i>Tumor stage</i>						
Stage I and II	121 (0.48)	132 (0.52)	0.728 (0.450–1.178)	0.196	-	-
Stage III and IV	51 (0.60)	34 (0.40)	0.323 (0.167–0.625)	0.001	-	-
Missing	9	15				
<i>BMI (kg/m<sup>2</sup>)</i>						
< 18.5	15 (0.71)	6 (0.29)	0.849 (0.093–7.734)	0.884	0.000 (0–6.320E+148)	0.947
18.5–24.9	85 (0.55)	69 (0.45)	0.288 (0.151–0.549)	0.000	0.305 (0.156–0.596)	0.001
25–29.9	45 (0.51)	43 (0.49)	0.568 (0.267–1.209)	0.142	0.422 (0.179–0.998)	0.049
≥ 30	23 (0.34)	45 (0.66)	0.955 (0.401–2.272)	0.917	1.082 (0.428–2.738)	0.868
Missing	13	18				

\*Adjusted for tumor stage of TCGA; MST, median survival time; No. of events, number of events; HR, hazard ratio; CI, confidence interval; OS, overall survival

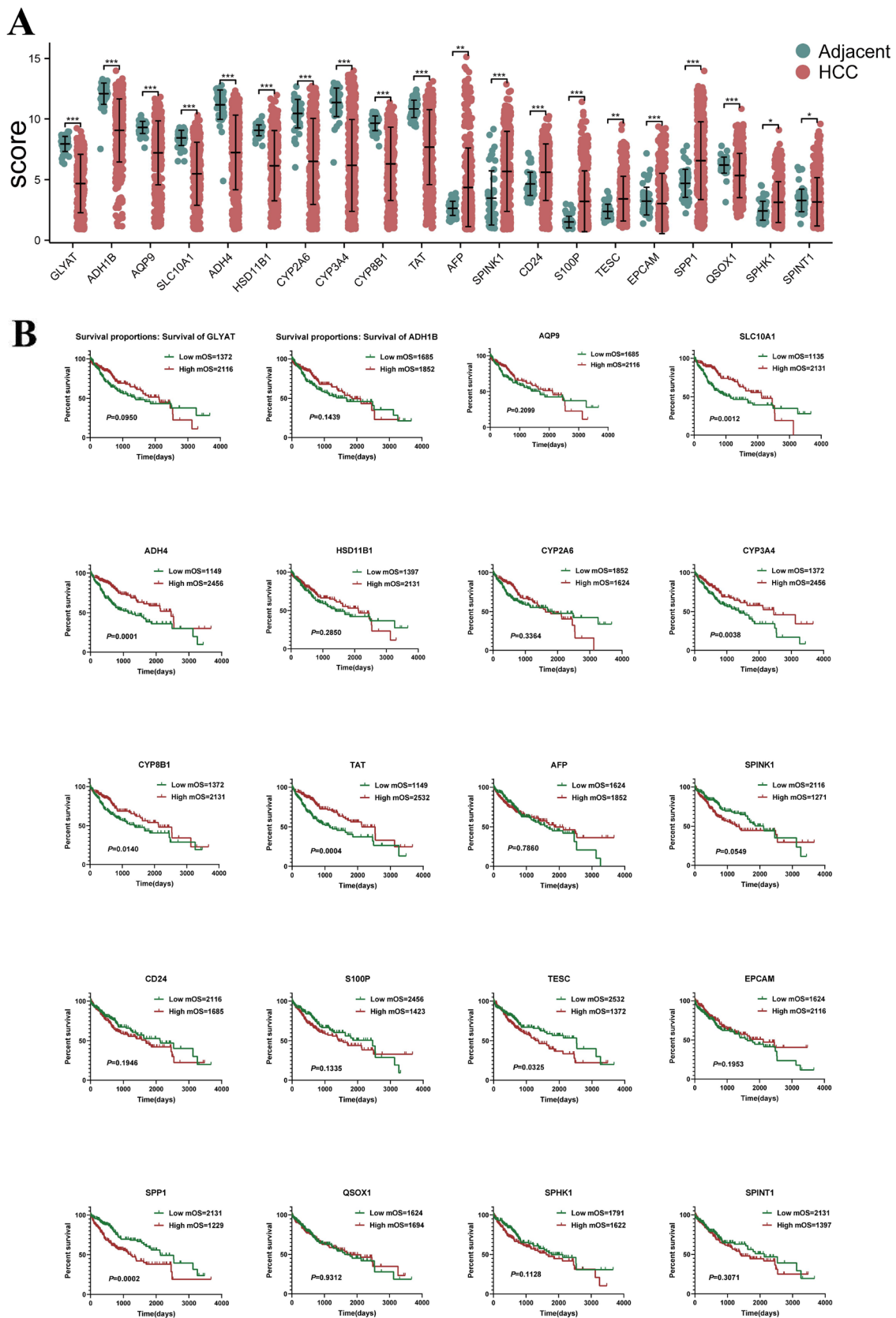


**Fig. 6** **A** Expression of 20 DEGs in hepatocellular carcinoma tissues and normal tissues. \*\*\* $P < 0.001$ , \*\* $P < 0.01$ , \* $P < 0.05$ . **B** Kaplan–Meier survival analysis for 20 DEGs

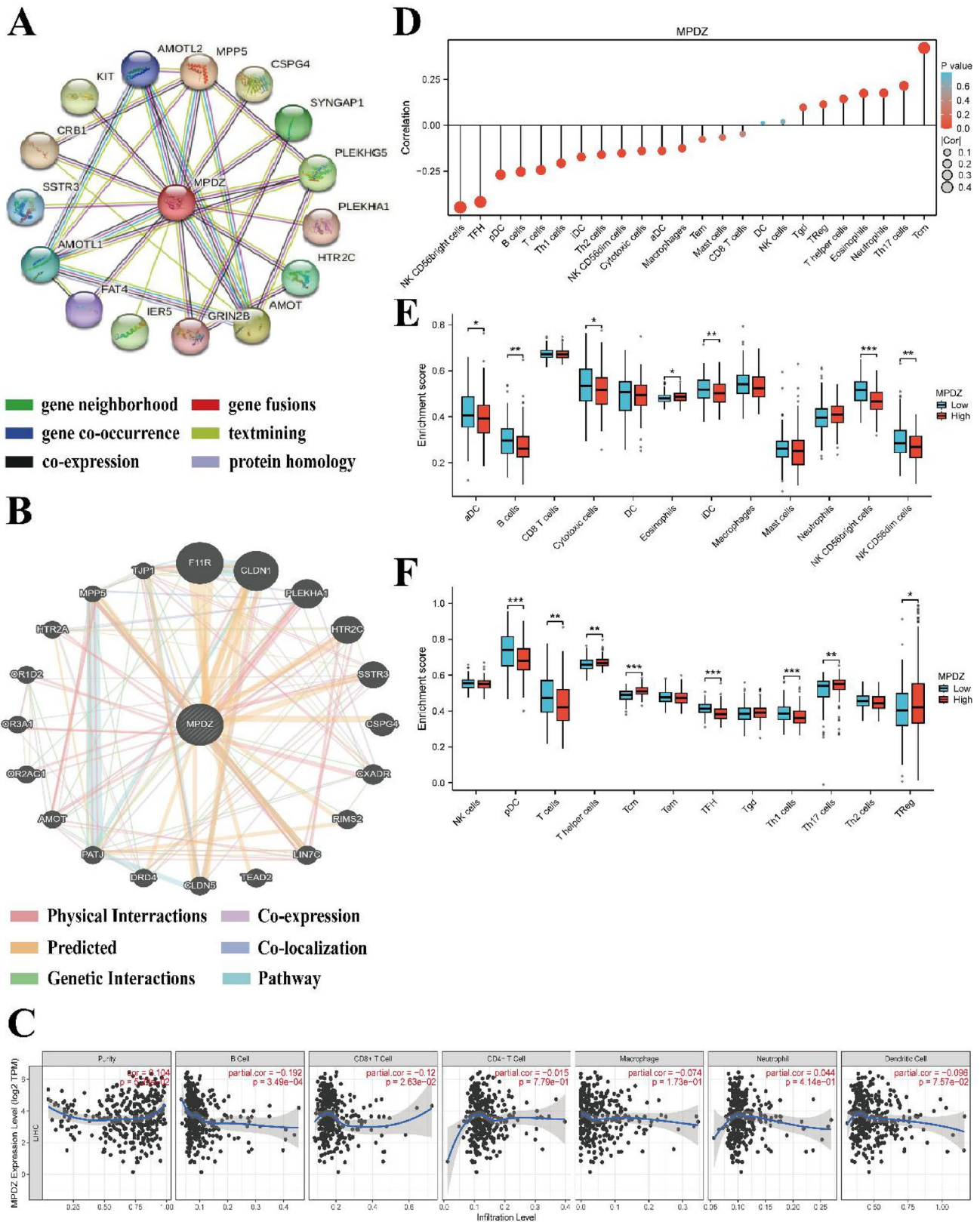


**Fig. 7** **A** protein–protein interaction network of MPDZ in STRING; **B** gene–gene interaction network of MPDZ in GeneMANIA; **C** correlation of MPDZ expression with tumor-infiltrating immune cells;

**D** bubble plots showing the correlation between MPDZ and different immune cells; **E**, **F** violin plots showing the degree of infiltration of different immune cells in the MPDZ<sup>high</sup> and MPDZ<sup>low</sup> groups

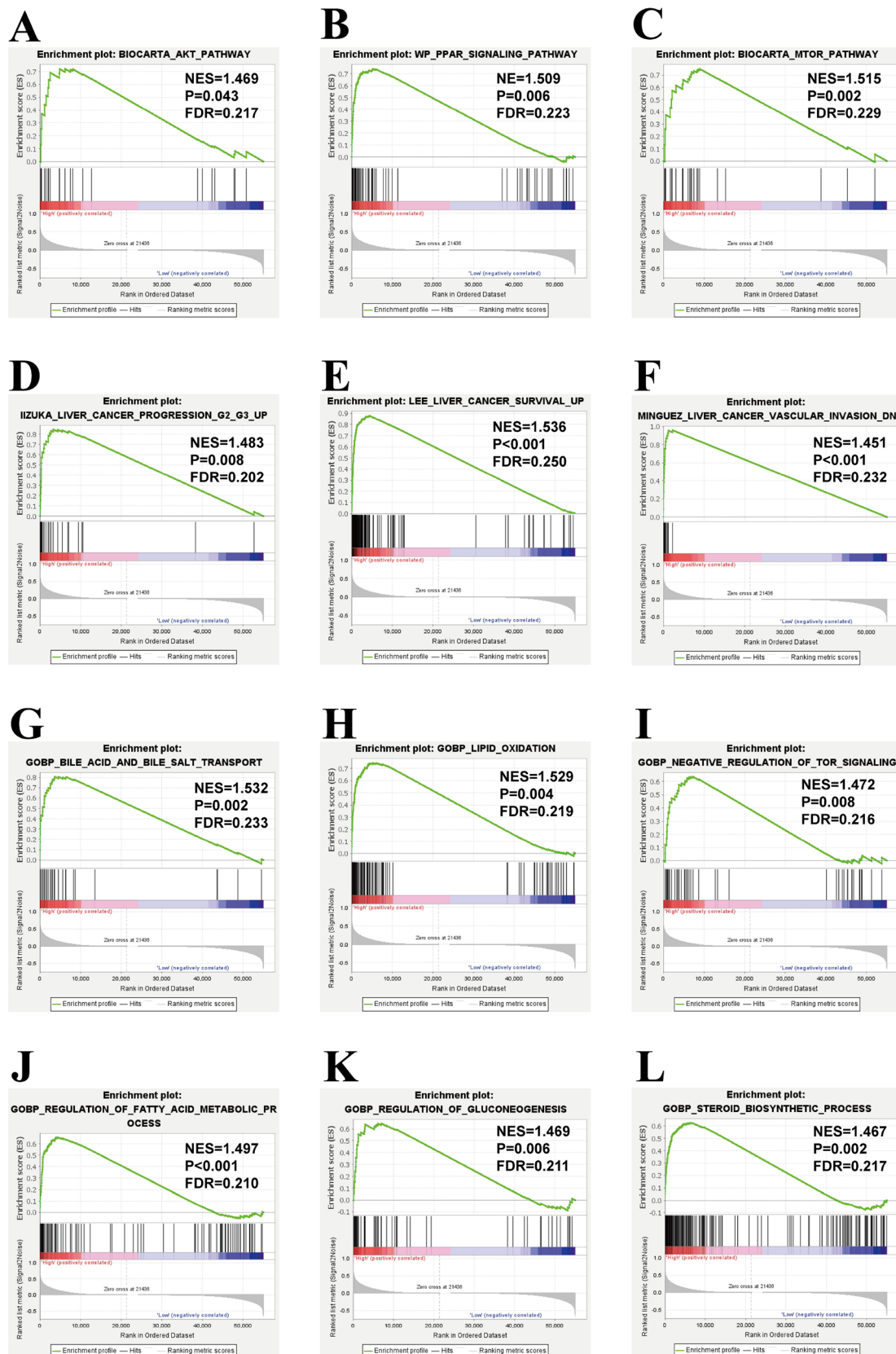


**Fig. 8** A–F GSEA results for the c2 reference genome of MPDZ; G–L GSEA results for the c5 reference genome of CST7. ES, enrichment score; FDR q-val, false discovery rate q-value; NOM p-val, nominal *P* value

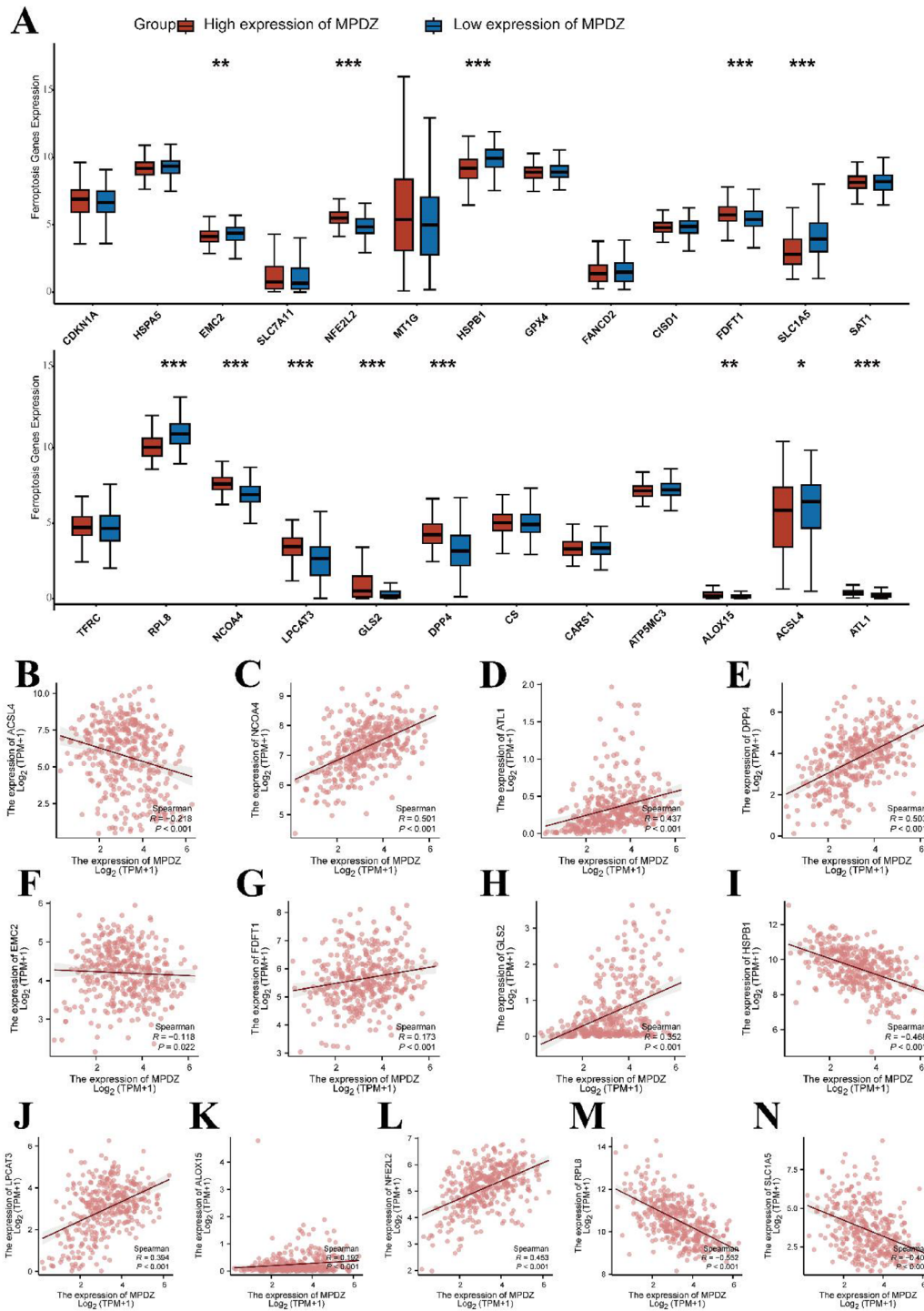


**Fig. 9** A Expression of ferroptosis-related genes in the high and low MPDZ expression groups; B–N Scatter plot of correlation between MPDZ expression and 13 ferroptosis-related genes that were differ-

entially expressed in the MPDZ high and ground expression groups. \* $P < 0.05$ , \*\* $P < 0.01$ , \*\*\* $P < 0.001$

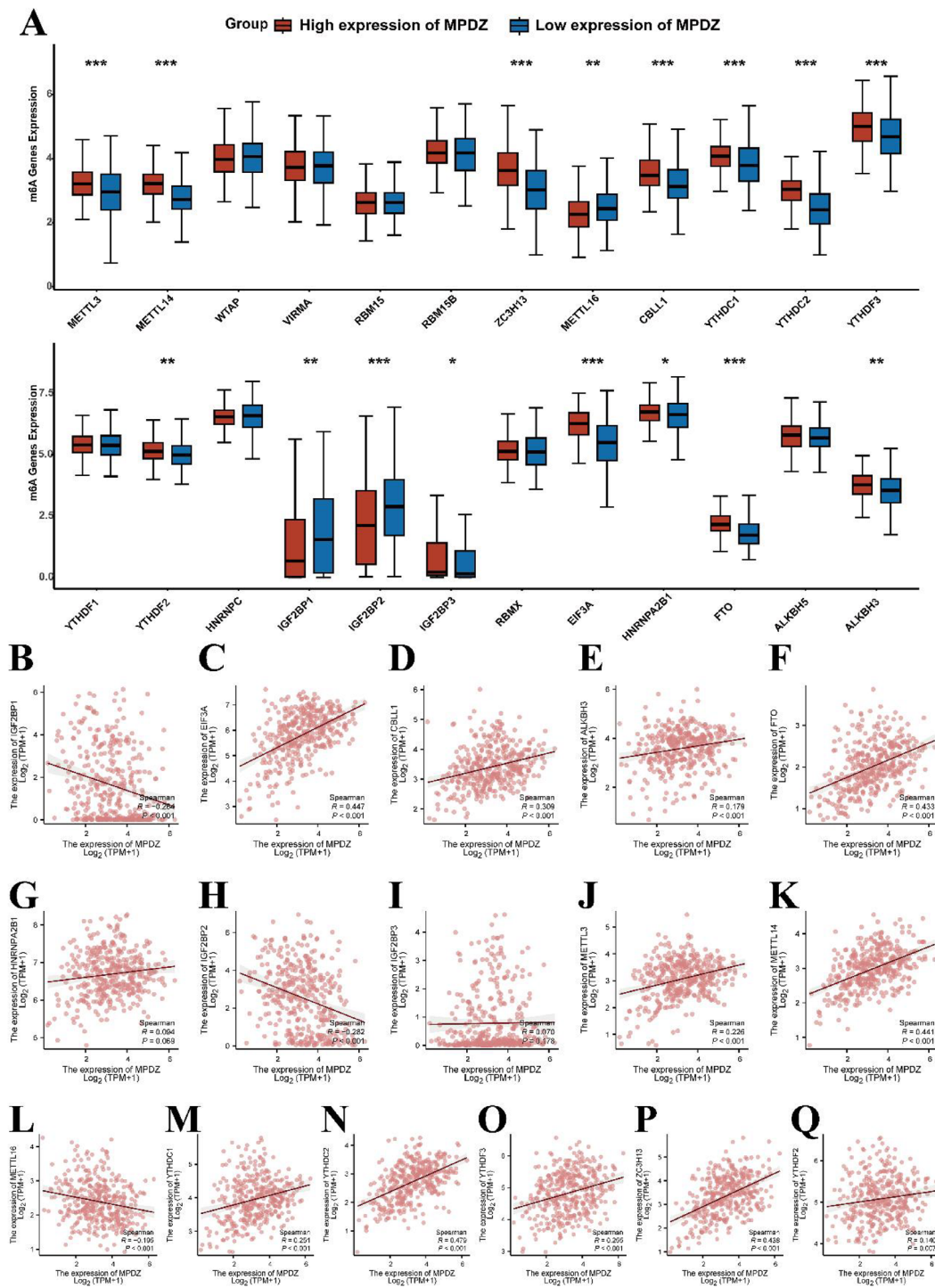


**Fig. 10** A Expression of m6A-related genes in the high and low MPDZ expression groups; B–Q Scatter plot of correlation between MPDZ expression and 16 m6A-related genes that were differen-

tially expressed in the MPDZ high and ground expression groups. \**P* < 0.05, \*\**P* < 0.01, \*\*\**P* < 0.001

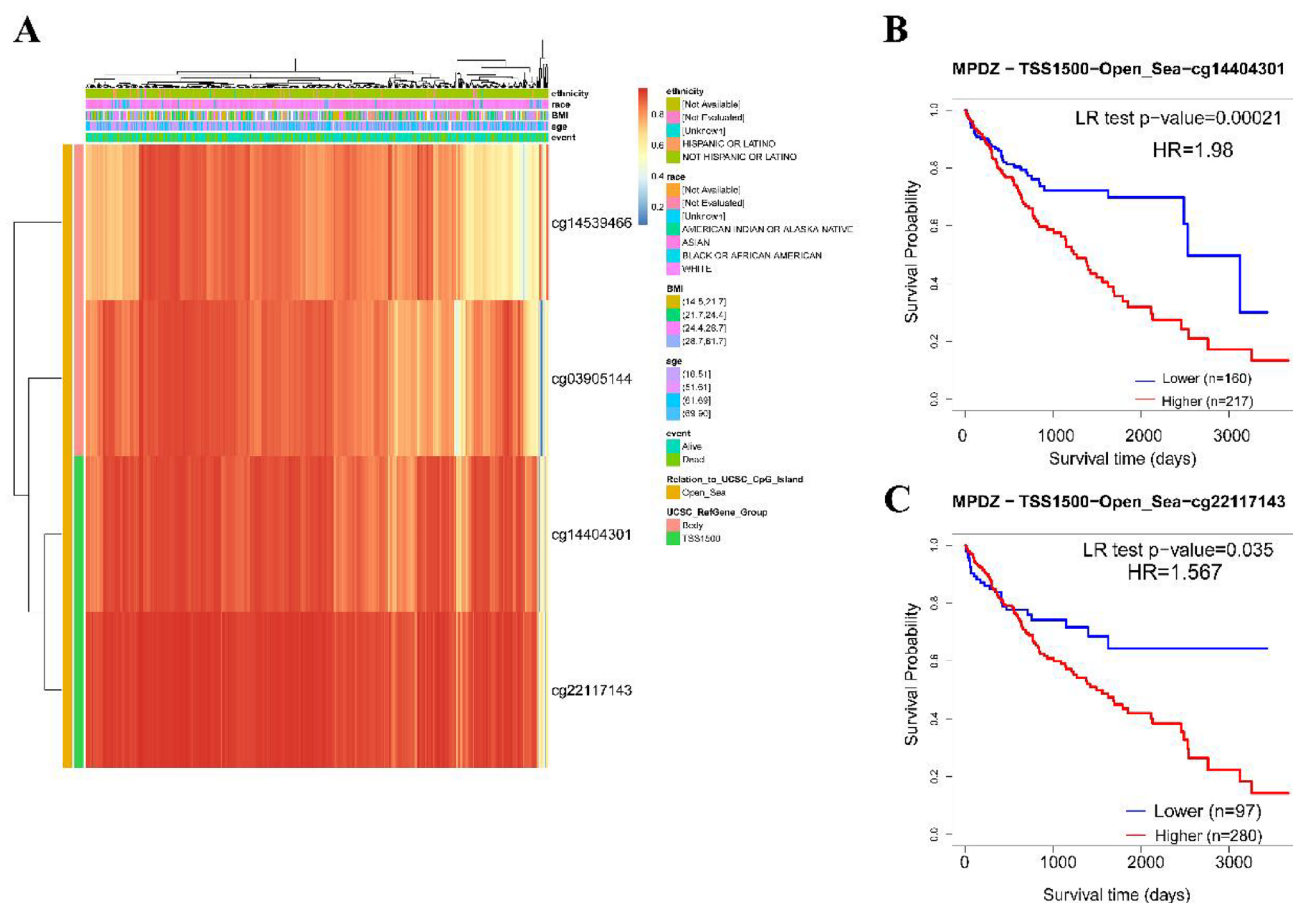


**Fig. 11** A Correlation between MPDZ expression levels and methylation levels and their clinical features. **B, C** Kaplan–Meier curves of two methylation sites in MPDZ

In contrast to the tissues of the normal liver, MPDZ is downregulated in the tissues of HCC and portends a worse prognosis. MPDZ is a novel biomarker for the diagnosis and prognosis of HCC.

**Acknowledgements** The authors are grateful to these databases (GSE14520, GSE62232, GSE76427, GSE121248, GSE136247, TCGA) for providing data related to hepatocellular carcinoma.

**Authors' contributions** All authors contributed to the study conception and design. J.Z L and J.H L conceived and designed the manuscript, material preparation, data collection, and analysis were performed by H.X X, X.Q S, F.Q. Y, and J.G C. T.M L guided and supervised the manuscript. The first draft of the manuscript was written by J.Z L and all authors commented on previous versions of the manuscript. All authors read and approved the final manuscript.

**Funding** The research was supported by the Open Project of Guangxi Key Laboratory of Enhanced Recovery after Surgery for Gastrointestinal Cancer (GXEKL202405) and Huaier Special Fund for Cancer Prevention and Control in 2024 (Hubei Chen Xiaoping Science and Technology Development Foundation, CXPJH124009-004).

**Data availability** No datasets were generated or analyzed during the current study.

## Declarations

**Conflict of interest** The authors declare no competing interests.

**Ethics approval and consent to participate** This study had acquired the approval of the Ethics Committee of the first affiliated hospital of Guangxi Medical University before specimen collection was conducted in line with the Declaration of Helsinki. Approval Number: no. 2023-E535-01.

**Patient consent for publication** Not applicable.

**Open Access** This article is licensed under a Creative Commons Attribution-NonCommercial-NoDerivatives 4.0 International License, which permits any non-commercial use, sharing, distribution and reproduction in any medium or format, as long as you give appropriate credit to the original author(s) and the source, provide a link to the Creative Commons licence, and indicate if you modified the licensed material. You do not have permission under this licence to share adapted material

derived from this article or parts of it. The images or other third party material in this article are included in the article's Creative Commons licence, unless indicated otherwise in a credit line to the material. If material is not included in the article's Creative Commons licence and your intended use is not permitted by statutory regulation or exceeds the permitted use, you will need to obtain permission directly from the copyright holder. To view a copy of this licence, visit <http://creativecommons.org/licenses/by-nc-nd/4.0/>.

## References

- Sung H, Ferlay J, Siegel RL, et al. Global cancer statistics 2020: GLOBOCAN estimates of incidence and mortality worldwide for 36 cancers in 185 countries. *CA A Cancer J Clin*. 2021;71(3):209–49.
- Bray F, Ferlay J, Soerjomataram I, et al. Global cancer statistics 2018: GLOBOCAN estimates of incidence and mortality worldwide for 36 cancers in 185 countries. *CA Cancer J Clin*. 2018;68(6):394–424.
- Zhang C-H, Cheng Y, Zhang S, et al. Changing epidemiology of hepatocellular carcinoma in Asia. *Liver Int*. 2022;42(9):2029–41.
- Vogel A, Saborowski A. Medical therapy of HCC. *J Hepatol*. 2022;76(1):208–10.
- Yang JD, Hainaut P, Gores GJ, et al. A global view of hepatocellular carcinoma: trends, risk, prevention and management. *Nat Rev Gastroenterol Hepatol*. 2019;16(10):589–604.
- Wang W, Wei C. Advances in the early diagnosis of hepatocellular carcinoma. *Genes Dis*. 2020;7(3):308–19.
- Tsuchiya N, Sawada Y, Endo I, et al. Biomarkers for the early diagnosis of hepatocellular carcinoma. *World J Gastroenterol*. 2015;21(37):10573–83.
- Siegel RL, Miller KD, Fuchs HE, et al. Cancer statistics, 2021. *CA Cancer J Clin*. 2021. <https://doi.org/10.3322/caac.21654>.
- Gupta S, Bent S, Kohlwes J. Test characteristics of alpha-fetoprotein for detecting hepatocellular carcinoma in patients with hepatitis C. A systematic review and critical analysis. *Ann Intern Med*. 2003;139(1):46–50.
- Trevisani F, D'Intino PE, Morselli-Labate AM, et al. Serum alpha-fetoprotein for diagnosis of hepatocellular carcinoma in patients with chronic liver disease: influence of HBsAg and anti-HCV status. *J Hepatol*. 2001;34(4):570–5.
- Tzartzeva K, Obi J, Rich NE, et al. Surveillance imaging and alpha fetoprotein for early detection of hepatocellular carcinoma in patients with cirrhosis: a meta-analysis. *Gastroenterology*. 2018. <https://doi.org/10.1053/j.gastro.2018.01.064>.
- Ullmer C, Schmuck K, Figge A, et al. Cloning and characterization of MUPP1, a novel PDZ domain protein. *FEBS Lett*. 1998;424(1–2):63–8.
- Adachi M, Hamazaki Y, Kobayashi Y, et al. Similar and distinct properties of MUPP1 and Patj, two homologous PDZ domain-containing tight-junction proteins. *Mol Cell Biol*. 2009;29(9):2372–89.
- Hamazaki Y, Itoh M, Sasaki H, et al. Multi-PDZ domain protein 1 (MUPP1) is concentrated at tight junctions through its possible interaction with claudin-1 and junctional adhesion molecule. *J Biol Chem*. 2002;277(1):455–61.
- Ernkvist M, Luna Persson N, Audebert S, et al. The Amot/Patj/Syx signaling complex spatially controls RhoA GTPase activity in migrating endothelial cells. *Blood*. 2009;113(1):244–53.
- Feldner A, Adam MG, Tetzlaff F, et al. Loss of Mpdz impairs ependymal cell integrity leading to perinatal-onset hydrocephalus in mice. *EMBO Mol Med*. 2017;9(7):890–905.
- Sitek B, Poschmann G, Schmidtke K, et al. Expression of MUPP1 protein in mouse brain. *Brain Res*. 2003;970(1–2):178–87.
- Lun MP, Monuki ES, Lehtinen MK. Development and functions of the choroid plexus-cerebrospinal fluid system. *Nat Rev Neurosci*. 2015;16(8):445–57.
- Spector R, Keep RF, Robert Snodgrass S, et al. A balanced view of choroid plexus structure and function: focus on adult humans. *Exp Neurol*. 2015;267:78–86.
- Yang J, Simonneau C, Kilker R, et al. Murine MPDZ-linked hydrocephalus is caused by hyperpermeability of the choroid plexus. *EMBO Mol Med*. 2019, 11(1).
- Guillaume J-L, Daulat AM, Maurice P, et al. The PDZ protein muppl1 promotes Gi coupling and signaling of the Mtl melatonin receptor. *J Biol Chem*. 2008;283(24):16762–71.
- Krapivinsky G, Medina I, Krapivinsky L, et al. SynGAP-MUPP1-CaMKII synaptic complexes regulate p38 MAP kinase activity and NMDA receptor-dependent synaptic AMPA receptor potentiation. *Neuron*. 2004;43(4):563–74.
- Tetzlaff F, Adam MG, Feldner A, et al. MPDZ promotes DLL4-induced Notch signaling during angiogenesis. *Elife*. 2018. <https://doi.org/10.7554/eLife.32860>.
- Coyne CB, Voelker T, Pichla SL, et al. The coxsackievirus and adenovirus receptor interacts with the multi-PDZ domain protein-1 (MUPP-1) within the tight junction. *J Biol Chem*. 2004;279(46):48079–84.
- Martin TA, Watkins G, Mansel RE, et al. Loss of tight junction plaque molecules in breast cancer tissues is associated with a poor prognosis in patients with breast cancer. *Eur J Cancer*. 2004;40(18):2717–25.
- Massimi P, Gammoh N, Thomas M, et al. HPV E6 specifically targets different cellular pools of its PDZ domain-containing tumour suppressor substrates for proteasome-mediated degradation. *Oncogene*. 2004;23(49):8033–9.
- Yuan C, Yuan M, Chen M, et al. Prognostic implication of a novel metabolism-related gene signature in hepatocellular carcinoma. *Front Oncol*. 2021;11: 666199.
- Kamarudin AN, Cox T, Kolamunnage-Dona R. Time-dependent ROC curve analysis in medical research: current methods and applications. *BMC Med Res Methodol*. 2017;17(1):53.
- Balachandran VP, Gonen M, Smith JJ, et al. Nomograms in oncology: more than meets the eye. *Lancet Oncol*. 2015;16(4):e173–80.
- Heagerty PJ, Zheng Y. Survival model predictive accuracy and ROC curves. *Biometrics*. 2005. <https://doi.org/10.1111/j.0006-341X.2005.030814.x>.
- He Q, Yang J, Jin Y. Immune infiltration and clinical significance analyses of the coagulation-related genes in hepatocellular carcinoma. *Brief Bioinform*. 2022. <https://doi.org/10.1093/bib/bbac291>.
- Deng M, Sun S, Zhao R, et al. The pyroptosis-related gene signature predicts prognosis and indicates immune activity in hepatocellular carcinoma. *Mol Med*. 2022;28(1):16.
- Pontén F, Jirstrom K, Uhlen M. The Human Protein Atlas—a tool for pathology. *J Pathol*. 2008;216(4):387–93.
- Szklarczyk D, Gable AL, Nastou KC, et al. The STRING database in 2021: customizable protein-protein networks, and functional characterization of user-uploaded gene/measurement sets. *Nucleic Acids Res*. 2021;49(D1):D605–12.
- Franz M, Rodriguez H, Lopes C, et al. GeneMANIA update 2018. *Nucleic Acids Res*. 2018;46(W1):W60–4.
- Liberzon A, Birger C, Thorvaldsdottir H, et al. The molecular signatures database (MSigDB) hallmark gene set collection. *Cell Syst*. 2015;1(6):417–25.
- Expansion of the Gene Ontology knowledgebase and resources. *Nucleic Acids Res*. 45(D1): D331–D8.

38. Kanehisa M, Furumichi M, Tanabe M, et al. KEGG: new perspectives on genomes, pathways, diseases and drugs. *Nucleic Acids Res.* 2017;45(D1):D353–61.
39. Modhukur V, Ijjasenko T, Metsalu T, et al. MethSurv: a web tool to perform multivariable survival analysis using DNA methylation data. *Epigenomics.* 2018;10(3):277–88.
40. Iseda N, Itoh S, Toshida K, et al. Ferroptosis is induced by lenvatinib through fibroblast growth factor receptor-4 inhibition in hepatocellular carcinoma. *Cancer Sci.* 2022;113(7):2272–87.
41. Zhang L, Li XM, Shi XH, et al. Sorafenib triggers ferroptosis via inhibition of HBXIP/SCD axis in hepatocellular carcinoma. *Acta Pharmacol Sin.* 2023;44(3):622–34.
42. Chen S, Xia H, Sheng L. WTAP-mediated m6A modification on circCMTM3 inhibits hepatocellular carcinoma ferroptosis by recruiting IGF2BP1 to increase PARK7 stability. *Dig Liver Dis.* 2023;55(7):967–81.
43. Liu Z, Zhao Q, Zuo ZX, et al. Systematic analysis of the aberrances and functional implications of ferroptosis in cancer. *iScience.* 2020;23(7): 101302.
44. Li Y, Xiao J, Bai J, et al. Molecular characterization and clinical relevance of m(6)A regulators across 33 cancer types. *Mol Cancer.* 2019;18(1):137.
45. Wang Z, Jensen MA, Zenklusen JC. A practical guide to the cancer genome atlas (TCGA). *Methods Mol Biol.* 2016;1418:111–41.
46. Kudo M, Finn RS, Qin S, et al. Lenvatinib versus sorafenib in first-line treatment of patients with unresectable hepatocellular carcinoma: a randomised phase 3 non-inferiority trial. *Lancet.* 2018;391(10126):1163–73.
47. Cheng A-L, Hsu C, Chan SL, et al. Challenges of combination therapy with immune checkpoint inhibitors for hepatocellular carcinoma. *J Hepatol.* 2020;72(2):307–19.
48. Finn RS, Ryoo B-Y, Merle P, et al. Pembrolizumab as second-line therapy in patients with advanced hepatocellular carcinoma in KEYNOTE-240: a randomized, double-blind, phase III trial. *J Clin Oncol.* 2020;38(3):193–202.
49. Kruse LC, Walter NAR, Buck KJ. Mpdz expression in the caudolateral substantia nigra pars reticulata is crucially involved in alcohol withdrawal. *Genes Brain Behav.* 2014;13(8):769–76.
50. Fehr C, Shirley RL, Metten P, et al. Potential pleiotropic effects of Mpdz on vulnerability to seizures. *Genes Brain Behav.* 2004. <https://doi.org/10.1111/j.1601-183X.2004.00035.x>.
51. Liu W, Huang Y, Wang D, et al. MPDZ as a novel epigenetic silenced tumor suppressor inhibits growth and progression of lung cancer through the Hippo-YAP pathway. *Oncogene.* 2021;40(26):4468–85.
52. Huang Y-S, Liu W-B, Han F, et al. Copy number variations and expression of MPDZ are prognostic biomarkers for clear cell renal cell carcinoma. *Oncotarget.* 2017;8(45):78713–25.
53. Chanez B, Appay R, Guille A, et al. Genomic analysis of paired IDHwt glioblastomas reveals recurrent alterations of MPDZ at relapse after radiotherapy and chemotherapy. *J Neurol Sci.* 2022;436: 120207.
54. Wu L, Zhang X, Zheng L, et al. RIPK3 orchestrates fatty acid metabolism in tumor-associated macrophages and hepatocarcinogenesis. *Cancer Immunol Res.* 2020;8(5):710–21.
55. Liu D, Wong CC, Fu L, et al. Squalene epoxidase drives NAFLD-induced hepatocellular carcinoma and is a pharmaceutical target. *Sci Transl Med.* 2018. <https://doi.org/10.1126/scitranslmed.aap9840>.
56. Cao F, Luo A, Yang C. G6PD inhibits ferroptosis in hepatocellular carcinoma by targeting cytochrome P450 oxidoreductase. *Cell Signal.* 2021;87: 110098.
57. Feng J, Dai W, Mao Y, et al. Simvastatin re-sensitizes hepatocellular carcinoma cells to sorafenib by inhibiting HIF-1 $\alpha$ /PPAR- $\gamma$ /PKM2-mediated glycolysis. *J Exp Clin Cancer Res.* 2020;39(1):24.
58. Arechederra M, Bazai SK, Abdouni A, et al. ADAMTSL5 is an epigenetically activated gene underlying tumorigenesis and drug resistance in hepatocellular carcinoma. *J Hepatol.* 2021;74(4):893–906.
59. Du D, Liu C, Qin M, et al. Metabolic dysregulation and emerging therapeutic targets for hepatocellular carcinoma. *Acta Pharm Sin B.* 2022;12(2):558–80.
60. Zhou C, Liu C, Liu W, et al. SLFN11 inhibits hepatocellular carcinoma tumorigenesis and metastasis by targeting RPS4X via mTOR pathway. *Theranostics.* 2020;10(10):4627–43.
61. Chen J, Ding C, Chen Y, et al. Acs14 reprograms fatty acid metabolism in hepatocellular carcinoma via c-Myc/SREBP1 pathway. *Cancer Lett.* 2021;502:154–65.
62. Xu D, Wang Z, Xia Y, et al. The gluconeogenic enzyme PCK1 phosphorylates INSIG1/2 for lipogenesis. *Nature.* 2020;580(7804):530–5.
63. Sun R, Zhang Z, Bao R, et al. Loss of SIRT5 promotes bile acid-induced immunosuppressive microenvironment and hepatocarcinogenesis. *J Hepatol.* 2022;77(2):453–66.
64. Luo X, Zheng E, Wei L, et al. The fatty acid receptor CD36 promotes HCC progression through activating Src/PI3K/AKT axis-dependent aerobic glycolysis. *Cell Death Dis.* 2021;12(4):328.
65. Zhu X, Sha X, Zang Y, et al. Current progress of ferroptosis study in hepatocellular carcinoma. *Int J Biol Sci.* 2024;20(9):3621–37.
66. Xu RH, Wei W, Krawczyk M, et al. Circulating tumour DNA methylation markers for diagnosis and prognosis of hepatocellular carcinoma. *Nat Mater.* 2017;16(11):1155–61.
67. Ma H, Hong Y, Xu Z, et al. N(6)-methyladenosine (m(6)A) modification in hepatocellular carcinoma. *Biomed Pharmacother.* 2024;173: 116365.

**Publisher's Note** Springer Nature remains neutral with regard to jurisdictional claims in published maps and institutional affiliations.